A Comparative Study on Mesoporous Y Zeolites Prepared by Hard-Templating and Post-Synthetic Treatment Methods

Samer Abdulridha [a, b], Yilai Jiao [a, c], Shaojun Xu [a], Rongxin Zhang [a], Zhongyuan Ren [d], Arthur A. Garforth [a], Xiaolei Fan [a, *]

[a] Department of Chemical Engineering and Analytical Science, School of Engineering, The University of Manchester, Manchester, M13 9PL, United Kingdom
[b] Petroleum Research and Development Center, Ministry of Oil, Baghdad, Iraq
[c] Shenyang National Laboratory for Materials Science, Institute of Metal Research, Chinese Academy of Sciences, 72 Wenhua Road, Shenyang, 110016, China
[d] Jilin Institute of Chemical Technology, No. 45 Chengde Street, Jilin, China

ARTICLE INFO

Keywords:
Mesoporous zeolites
zeolite Y
templating
post-synthetic treatment
catalytic cracking

ABSTRACT

Mesoporous Y zeolites were prepared comparatively using the bottom-up templating (with carbon nanotubes, CNTs, and nanocrystalline cellulose, NCC, as the templates) and the top-down post-synthetic treatment (with the sequential chemical and alkaline treatment) methods and characterised comprehensively using various techniques. The relevant findings show that the mesoporous Y zeolites with the intercrystal mesoporosity were prepared by the templating methods, and the NCC is the more effective, economic and sustainable hard template than the CNTs for promoting the formation of intercrystal mesoporosity. While for the post-synthetic strategy, the microwave (MW)-assisted chemical treatment (using ethylenediaminetetraacetic acid, EDTA, as the chemical agent for dealumination) was much more effective than the conventional hydrothermal (HT) treatment for introducing intracrystalline mesoporosity under the comparable condition, e.g. the external surface area: 287 m^2 g^{-1} by 1 min MW treatment *vs.* 205 m^2 g^{-1} by 6 h HT treatment. The prepared mesoporous Y zeolites, along with the parent Y, were assessed using the catalytic cracking of 1,3,5 triisopriopylbenzene (TiPBz). It was found that the well-developed intracrystalline mesoporosity promoted by the effective MW-assisted post-synthesis method is highly beneficial to the catalysis involving the bulky molecules, and accordingly showed the comparatively best catalytic performance (regarding the conversion and selectivity) among all zeolites under study in this work.

1. Introduction

Synthetic zeolites, representing an important class of microporous materials, are crystalline aluminosilicate solid acid catalysts with direct industrial relevance. Zeolites have been used in numerous industrial catalysis, especially petrochemical conversion processes such as fluid catalytic cracking (FCC), alkylation and isomerisation, due to their good hydrothermal stability, high surface area, strong acidity and shape selectivity [1–3]. In particular, the faujasite (FAU) Y zeolite, having a three dimensional pore structure with a window aperture of ~0.74 nm and a spherical supercage with a diameter of 1.3 nm [4,5], is the most important active additives in FCC catalysts for gasoline range organics [6]. One of the drawbacks of Y zeolite arises from its intrinsic micro-porosity, imposing the accessibility issue and diffusion limitation, and thus causing the low activity and/or deactivation, particularly in reactions involving bulky molecules [3,7]. Therefore, great efforts have been made by both industrial and academic communities to improve the accessibility of zeolites in order to sustain or improve their catalytic effectiveness [8–13]. To alleviate this particular problem associated with microporous zeolites, a class of mesoporous zeolites (or ideally, hierarchical zeolites) was proposed and developed. Mesoporous zeolites couple a secondary network of meso- and/or macro-porosity to the intrinsic micropores, improving mass transport and diffusion within the framework, while preserving the zeolitic properties to a large extent [1, 8]. A wide variety of strategies have been developed to make meso-porous zeolites. Typically, they can be categorised into two classes, *i.e.* (*i*) the 'bottom-up' approach including the templating methods using either hard templates (*e.g.* carbon nanostructures) [14,15] or soft tem-plates (*e.g.* cetyltrimethylammonium bromide, CTAB or block co-polymers) [16–19] and (*ii*) the 'top-down' approach comprising post-synthetic treatments of parent zeolites *via* dealumination and desilication [20–26]. Both strategies have pros and cons. For example,

* Corresponding author.
E-mail address: xiaolei.fan@manchester.ac.uk (X. Fan).

although the bottom-up approach is versatile and relatively controllable, the use of templates presents the cost and environmental issues, hindering their applications at scales [1]. Conversely, the top-down approach is relatively practical, whereas it is also energy-intensive and suffers from the loss of zeolitic materials (*i.e.* the yield loss) [1,27,28]. There are various types of the two approaches being developed inde-pendently to date, and a fair comparison between them is, therefore, very challenging.

In this work, we made an effort to perform a comparative study on mesoporous Y zeolites prepared by the selected bottom-up [19] and top-down [26] methods, aiming to provide some insights into the effectiveness of the two approaches for making mesoporous Y zeolites. In the bottom-up synthesis, the hard-templating method using two mesoscopic templates (*i.e.* carbon nanotubes (CNT) and nanocrystalline cellulose (NCC)) was employed to prepare mesoporous Y zeolites. In the top-down treatment, a sequential chemical (using ethyl-enediaminetetraacetic acid, EDTA) and alkaline (using sodium hydrox-ide, NaOH) treatment was employed to prepare mesoporous Y zeolites. Specially, in the first step chemical treatment of the parent Y zeolite, both the conventional hydrothermal treatment and the microwave-assisted treatment were used. Importantly, for all the four methods studied, the parent zeolite Y was prepared using the same synthesis method (in the bottom-up synthesis, hard templates were added before the crystallisation under the hydrothermal condition), accordingly, the comparison of the relevant outcomes is considered fair. The resulting mesoporous Y zeolites were characterised comparatively using various techniques, and their catalytic performance was evaluated by the catalytic cracking of 1,3,5 triisopropylbenzene (TiPBz). Addi-tionally, the effect of the hierarchal feature of the mesoporous Y zeolites on the catalytic cracking performance and products selectivity, as well as the preliminary economic analysis, were also discussed.

2. Experimental

2.1. Chemicals and materials

Chemicals and materials used in the synthesis of FAU Y and meso-porous Y zeolites include sodium aluminate (Al_2O_3, 55%; Na_2O, 45 %; Sigma-Aldrich), Ludox® (AS-40, 40 wt. % suspension in H_2O, Sigma-Aldrich), sodium hydroxide (NaOH, 99%, Sigma-Aldrich), ammonium nitrate (NH_4NO_3, ACS reagent ≥98%, Sigma-Aldrich), multiwalled carbon nanotubes (CNTs, ≥98% carbon basis, Sigma-Aldrich), nano-crystalline cellulose (NCC, 99%, CelluForce Inc. Canada), sodium hy-pochlorite (NaOCl, 99%, Sigma-Aldrich), ethylenediaminetetraacetic acid (EDTA, 99%, Sigma-Aldrich).

Chemicals used in GC calibration and catalytic tests are benzene (C_6H_6, ≥99.8%, Sigma-Aldrich), toluene ($C_6H_5CH_3$, ≥99.5%, Sigma-Aldrich), *para*-xylene ($C_6H_4(CH_3)_2$, ≥99.5% GC, Sigma-Aldrich), *ortho*-xylene ($C_6H_4(CH_3)_2$, ≥99.5% GC Sigma-Aldrich), *meta*-xylene ($C_6H_4(CH_3)_2$, ≥99.5% GC, Sigma-Aldrich), cumene (C_9H_{12} , 99%, Alfa Aesar), 1,2,3-trimethylbenzene ($C_6H_3(CH_3)_3$, ≥99.5%, neat, GC, Sigma-Aldrich), 1,2,4-trimethylbenzene ($C_6H_3(CH_3)_3$, 98%, Sigma-Aldrich), 1,3-diisopropylbenzene ($C_{12}H_{18}$, 96%, Sigma-Aldrich), 1,4-diisopropyl-benzene ($C_{12}H_{18}$, 99%, Alfa Aesar), 1,3,5-triisopropylbenzene ($C_{15}H_{24}$, 95%, Alfa Aesar). All chemicals were used as received without further purification.

2.2. Preparation of mesoporous Y zeolites

2.2.1. Templating (bottom-up) synthesis

Details of the methods have been reported previously [19]. In brief, before the templating synthesis of mesoporous Y zeolites, the multi-walled carbon nanotubes (CNTs) were pre-treated by oxidation to in-crease the hydrophilicity. In a typical procedure, 230 mg CNTs was added to 40 mL of sodium hypochlorite solution (28 mL H_2O + 12 mL NaOCl), and stirred at room temperature for 24 h, followed by filtration, washing (with deionised water) and drying at 110 °C overnight. Nano-crystalline cellulose (NCC) was used as received without any further treatment.

A secondary growth method was modified to prepare the meso-porous Y zeolites [19]. Specifically, a colloidal seed was prepared with a composition of 10.67 Na_2O: Al_2O_3: 10 SiO_2: 180 H_2O. In a typical preparation, sodium aluminate and sodium hydroxide were firstly dis-solved in distilled water. Ludox solution was then added dropwise to the prepared solution under stirring. The colloidal solution was aged stati-cally at 25 °C for 24 h for seeds formation.

In order to achieve a uniform dispersion of hard templates in the colloidal seeds, the following procedure was used in this work. Colloidal seeds were stirred vigorously first with a stirring speed adjusted so that the vortex formed was large enough to reach the tip of the stir bar. Under this condition, the hard template (with a mass ratio of NCC or CNTs to Si in the colloidal seed equal to one) was added in small aliquots into the vortex over 5 min. Then mixture suspension was sonicated for 15 min followed by mixing for 20 min. The seed/template gel was then aged again for 24 h at 25 °C.

The synthesis gel was prepared with a composition of 4.30 Na_2O : Al_2O_3 : 10 SiO_2 : 180 H_2O. For the secondary growth synthesis, The seeded gel was then added to the synthesis gel under vigorous stirring (overall gel composition = 4.62 Na_2O : Al_2O_3 : 10 SiO_2 : 180 H_2O) and transferred into an autoclave reactor with 50 mL PTFE liner and aged in the oil bath at 100 °C for crystallisation. After the synthesis of 48 hours, a solid phase and a clear liquid phase were obtained in the PTFE liner.

The as-prepared zeolites were calcined at 600 °C for 15 h using a heating rate of 2 °C min^{-1} to remove the hard templates. Samples were labelled as MY–*x*, where *x* refers to the hard templates of NCC or CNTs. Yield of the mesoporous Y zeolites by the templating methods was determined according to Eq. 1.

$$\text{Yield} = \frac{\text{Actual yield}}{\text{Theoretical yield}} \times 100\% \quad (1)$$

where actual yield is the dry mass of the as-made mesoporous Y zeolite, and theoretical yield is the calculated mass (4 g) based on the limiting reactant used in the preparation recipe.

2.2.2. Post-synthetic treatments

The parent Y zeolite used in the post-synthetic treatments was pre-pared using the secondary synthesis method described above (without adding any hard templates). The post-synthetic modification of the parent Y zeolite was performed sequentially using chemical and alkaline treatment. The chemical modification was performed to dealuminate Y zeolite using aqueous EDTA solutions facilitated by hydrothermal (HT) and microwave (MW)-assisted (i.e. MWAC) treatments, as detailed in our previous studies [22,23,26]. Subsequently, chemically-treated Y zeolites were washed in aqueous NaOH solution.

Dealumination under the hydrothermal condition was performed in a 250 mL round-bottom flask under reflux for 6 h (solution volume =80 mL, 0.1 M EDTA, zeolite-to-solution ratio =0.066 g mL^{-1}). In the MWAC treatment, the parent zeolite Y was modified in 0.1 M EDTA aqueous solution (solution volume =25 mL, zeolite-to-solution ratio =0.066 g mL^{-1}, in 35 ml Pyrex vessels using a CEM Discover SP microwave sys-tem) for 1 min at 150 W, 2.5 GHz and 100 °C. After the chemical treatment, the mixture was quenched using ice water bath and separated by centrifugation, washed using desionised water, and dried overnight at 70 °C. The resulting modified zeolites were treated using the same alkaline treatment protocol, *i.e.* in 0.2 M NaOH aqueous solution (under stirring at 500 rpm) at 65 °C (3.3 g of chemically treated zeolite per 100 mL of NaOH solution). Finally, the zeolite was washed thoroughly using desionised water and dried at 100 °C overnight. Samples from the post-synthesis treatments were labelled as MY–*y*, where *y* refers to the chemical treatment with MW for the microwave-assisted method and HT for the conventional hydrothermal method.

The yield of the prepared Y zeolites by post-synthesis treatments was calculated based on the comparison of the dry masses of the obtained mesoporous Y (from the post-synthetic treatments) and the relevant starting parent Y.

2.3. Characterisation of materials

Powder X-ray diffraction (PXRD) patterns of zeolites were collected on a Philips X'Pert X-ray diffractometer with the conditions of Cu$K\alpha_1$ radiation, λ =1.5406 Å, 40 kV, 40 mA, 5° < 2θ < 65°, 0.0167° step size. The relative crystallinity (RC) of the prepared MY zeolites was calcu-lated according to the ASTM standard.[29] The peaks at the 2 theta angels of 15.7°, 18.7°, 20.4°, 23.7°, 27.1°, 30.8°, 31.5° and 34.2° were used for the calculation of the relative crystallinity. The RC value of each sample was then calculated based on the following equation (Eq. 2):

$$RC = \frac{S_x}{S_r} \times 100\% \quad (2)$$

where S_x is the sum of the total area under the specified peaks for the sample, and S_r is the sum of the total area under the specified peaks for the reference parent Y zeolite.

Nitrogen (N_2) adsorption-desorption analysis was performed at 196 °C using a Micromeritics 3Flex Surface Characterisation Analyser. Prior to the N_2 physisorption measurement, ~100 mg sample was degassed at 350 ° C under vacuum overnight. The specific surface area of the zeolites was determined using the Brunauer-Emmett-Teller (BET) method. Mesopore size distribution analysis was performed using the Barrett-Joyner-Halenda (BJH) method on the adsorption branch of the isotherm. X-ray fluorescence (XRF) was performed using PANalytical minipal4 (PANalytical EDXRD) spectrometer operated at 30 kV and 1 mA. Scanning electron microscopy (SEM) and energy dispersive X-ray diffraction (EDX) were undertaken by a FEI Quanta 250 FEG-SEM using a work distance of 8–10 mm and an accelerating voltage of 15 kV. All samples were dispersed in acetone and dropped onto SEM studs, fol-lowed by platinum coating using an Emitech K550X sputter coater under vacuum (1×10^{-4} mbar). High resolution transmission electron mi-croscopy (HRTEM) micrographs were obtained on a FEI Tecnai G2 F20 electron microscope operated at 200 kV. Thermogravimetry analysis (TGA) and differential thermal analysis (DTA) were performed on TG analyser (Beijing Boyuan Science and Technology Development Co., Ltd) at heating rate of 5 °C min^{-1} from 20 to 600 °C in air (100 mL min^{-1}). Ammonia temperature programmed desorption (NH_3-TPD) measurements were performed to determine the acid strength and the amounts of acidic sites on the catalysts. NH_3-TPD was performed using a Micrometrics AutoChem II 2920 chemisorption analyser (100 mg sam-ple, 10 K min^{-1}, He flow rate = 30 cm^3 STP min^{-1}). Details of NH_3-TPD analysis is described elsewhere [30]. Fourier transforms infrared trans-mission spectroscopy (FT-IR) was performed in a Bruker Vertex 70 spectrometer with the red light emission from a Helium-Neon laser and the wide range MIR-FIR beam splitter and detector. The spectra were obtained at ambient temperature by 56 scans at 4 cm^{-1} resolution in the wavelength range of 400–1,200 cm^{-1}.

2.4. Catalytic experiments

Before catalysis, all zeolites (Na-form) were converted to their H-forms *via* ion exchange, which was achieved by three consecutive ion-exchange treatments using 0.1 M aqueous NH_4NO_3 solution (1 g Na-form Y zeolite in 100 mL solution at 25 °C for 8 h per treatment). Samples were washed using deionised water and dried at 110 °C over-night in between the ion exchange treatments. Finally, the ion-exchanged products was calcined in static air at 450 ° C for 5 h using a heating rate of 5 °C min^{-1} to give the H-form zeolites for catalysis.

Catalytic cracking of 1,3,5-triisopropylbenzene (TiPBz) over the Y zeolites was performed at 325 °C under atmospheric pressure using a pulse method [19]. Zeolites were pelletised (with ~250 mesh particle sizes) then loaded (~20 mg) in a borosilicate glass-tube liner (internal diameter, i.d. = 4 mm; outer diameter, o.d. = 6.3 mm; length = 72 mm, Restek). Deactivated glass wool (Restek) was used to hold the bed. Then the tube was inserted into the gas chromatograph (GC, Varian 3400) injector and heated to 325 °C. The catalyst was heated at 325 °C for 1 h before injections in order to remove the moisture. Manual injection of 0.2 μL of TiPBz was performed using an Agilant SGE syringe (Trajan, 0.5BNR-5BV/0.63) with helium (He) as the carrier gas. Reactants/-products from the cracking reaction were analysed online by the GC equipped with a flame ionisation detector (FID). Details of the GC method used are presented in the Supporting Information (SI, Table S1). The analysis time for each injection was approximately 30 min. The total time of 17 injections were about 9 hours.

3. Results and discussion

3.1. Comparison of the properties of the mesoporous Y zeolites

XRD patterns of the as-prepared Y and MY zeolites are shown in Fig. 1. All mesoporous Y zeolites under investigation showed compara-ble diffraction patterns corresponding to the typical FAU crystalline structure (as the simulated XRD pattern of Y zeolite), indicating that (*i*) MY zeolites by the bottom-up methods were successfully formed with pure crystalline Y phase (Fig. 1a) and (*ii*) the original Y phase was reserved to a large extent after the top-down treatments (Fig. 1b).

As shown in Fig. 2a, the RC values of MY-CNTs and MY-NCC were about 86% and 80%, respectively, confirming the formation Y zeolite phase via the bottom-up methods with the hard templates. Compara-tively, the samples prepared by the top-down methods shows higher RC values than that prepared by the bottom-up methods. The relative crystallinity of MY-HT and MY-MW was about 98% and 90%, respec-tively. Accordingly, based on the findings on the relative crystallinity of the materials, one can conclude that the relatively good preservation of Y zeolite structure could be achieved when the top-down strategy was used to create mesoporous structure in the parent Y zeolite.

Concerning the yield, in comparison with the parent Y, the MY samples prepared by the bottom-up methods (Fig. 2b) show the slightly lower yields at about 62%, suggesting that the addition of the hard templates during the synthesis could hinder the crystallisation under the hydrothermal condition, being in line with the previous findings [19]. The top-down methods compromise the microporous phase of the parent Y to create secondary mesopores [26]. The MY-MW showed a slightly higher yield of ~62% than that of MY-HT (about 57%), suggesting that the improved effectiveness by MW irradiation than the conventional HT method with much shorter treatment time (*i.e.* 1 min for the MW method *vs.* 6 h for the HT method) and the reduced loss of materials. This is due to the direct framework Al removal by reactions between EDTA and framework Al species under the MW condition without the lengthy hy-drolysis required as under the conventional hydrothermal conditions [26].

XRF analysis (Fig. 2c) shows that the bulk molar silicon-to-aluminium (Si/Al) ratio of the prepared reference parent Y zeolite was ~2.6, while that for the MY zeolites by the bottom-up methods was 2.8 (for MY-CNTs) and 2.9 (for MY-CNCs), respectively. Since the top-down methods involve the dealumination of the parent Y zeolite, their Si/Al ratios are relatively higher at about 3.2. The findings from the XRF analysis showed that the bulk Si/Al ratio of the resulting MY zeolites could be preserved to some extent (in comparison to the parent Y) from both the bottom-up or top-down methods for the purpose of meso-porosity creation.

N_2 adsorption-desorption isotherms of the as-prepared Y and MY zeolites are presented in Fig. 3. The parent Y shows the type I isotherm corresponding to its microporous nature [31]. Conversely, the MY zeo-lites from the hard-templating methods and post-synthetic treatments presents the typical IV behaviours with the H2 hysteresis loop,

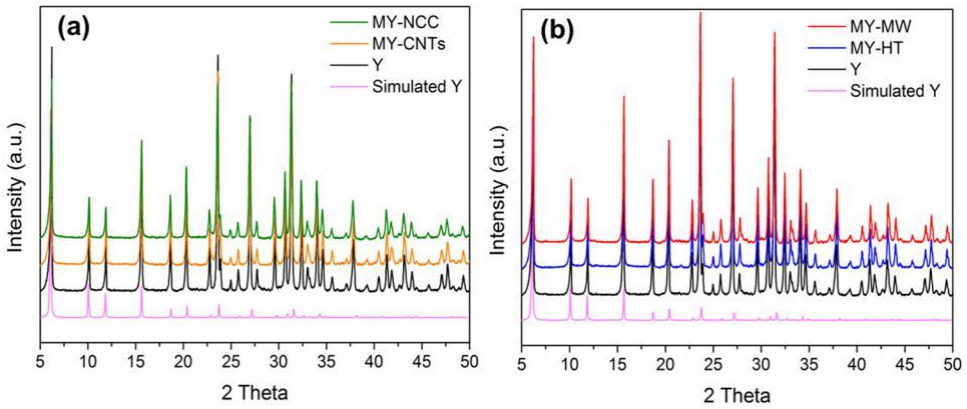

Fig. 1. XRD patterns of Y and MY zeolites prepared by this work in reference to the simulated XRD pattern of Y zeolite: (a) the zeolites prepared using the hard-templating method and (b) the zeolites prepared using the post-synthetic treatment methods.

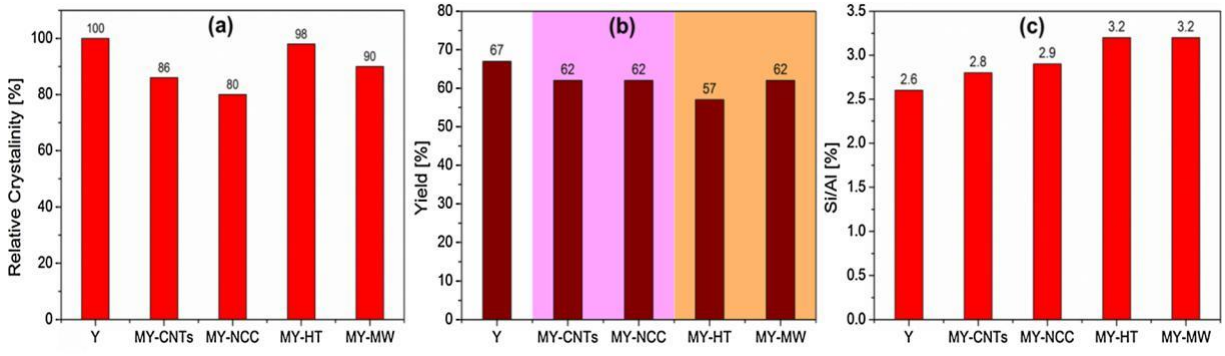

Fig. 2. (a) Relative crystallinity, (b) yield and (c) silicon-to-aluminium (Si/Al) ratio of the as-prepared Y zeolites.

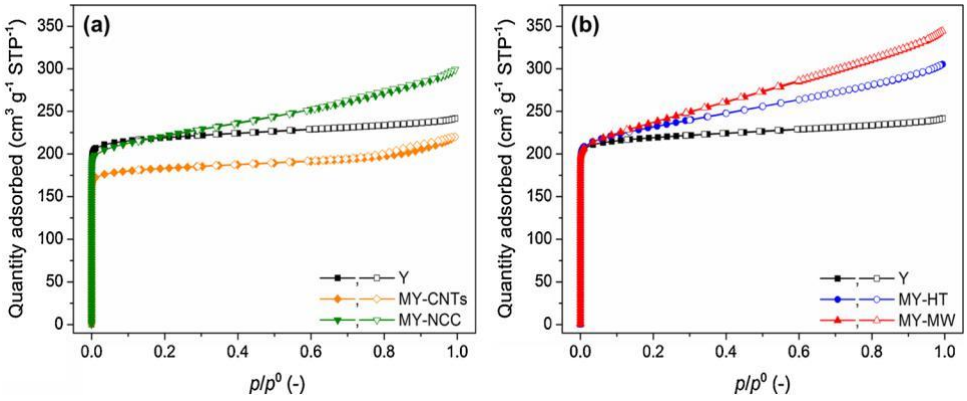

Fig. 3. N_2 adsorption-desorption isotherms of (a) the MY zeolites prepared by the templating methods and (b) the MY zeolites prepared by the post-synthesis treatments.

Table 1
Textural properties of the Y zeolites under investigation.

Sample	V_{total}[a] [$cm^3\ g^{-1}$]	V_{micro}[b] [$cm^3\ g^{-1}$]	V_{meso}[c] [$cm^3\ g^{-1}$]	S_{BET} [$m^2\ g^{-1}$]	S_{micro}[b] [$m^2\ g^{-1}$]	$S_{external}$[b] [$m^2\ g^{-1}$]	Avg. pore size[d] [nm]
Y	0.35	0.32	0.03	817	782	35	1.8
MY-CNTs	0.34	0.25	0.09	683	614	69	1.9
MY-NCC	0.46	0.25	0.21	814	617	197	2.2
MY-HT	0.47	0.26	0.21	854	649	205	2.2
MY-MW	0.53	0.24	0.29	865	578	287	2.4

[a] Total volume adsorbed at $p/p^0 = 0.99$.

[b] Based on the *t*-plot method.

[c] $V_{meso} = V_{total} - V_{micro}$.

[d] Adsorption average pore diameter.

suggesting the presence of mesopores in these materials. The textural property of the materials prepared by this work is summarised in Table 1. The parent Y shows insignificant mesoporous features con-cerning the specific external surface area ($S_{external}$) and specific meso-pore volume (V_{meso}). The templating method using CNTs seems to be less effective than that using the NCC template, producing the MY-CNTs with V_{meso} = 0.09 $cm^3\ g^{-1}$ and $S_{external}$ = 69 $m^2\ g^{-1}$. Considering the threshold value for mesoporous Y zeolites (*i.e.* V_{meso} >0.1 $cm^3\ g^{-1}$), the result of MY-CNTs is not satisfactory. Conversely, MY-NCC presents the relatively significant mesoporous features with V_{meso} = 0.21 $cm^3\ g^{-1}$ and $S_{external}$ = 197 $m^2\ g^{-1}$. By comparing the MY zeolites from the templating methods, apparently, CNTs are not very effective to produce mesopores which might be due to the phase separation issue, jeopard-ising the efficiency of templates utilisation [32], though the surface hydrophilicity of CNTs was adjusted *via* chemical oxidation. As a renewable and sustainable material, NCC did not to impose the phase separation problem in the synthesis protocol used by this work due to and the presence of the active surface of hydroxyl groups [19,33].

The separation issue might also induce the crystallisation difficulty during the hydrothermal synthesis, which is reflected by the BET surface area of the relevant MY zeolites (*i.e.* 683 $m^2\ g^{-1}$ for MY-CNTs and 814 $m^2\ g^{-1}$ for MY-NCC). The similar issue was also reported by Qiu *et al.*, in which the crystallisation of hierarchical HZSM-5 was hindered by the addition of CNTs [14]. The addition of the hard template reduced the rate of crystallisation, and hence the synthesis mesoporous ZSM-5 took 50% longer crystallisation time than the synthesis of normal HZSM-5. Comparatively, the NCC template shows much better compatibility than CNTs during the synthesis, resulting in the mesoporous zeolite Y (MY-NCC) with similar BET surface area to the parent Y.

In comparison with the hard-templating methods, the post-synthetic protocol was more effective to produce mesoporous Y zeolites with comparatively improved mesoporous features (as shown in Table 1). MY-NCC (by hard templating) and MY-HT (by post-synthetic treatment) shows comparable mesoporous features. For example, regarding the $S_{external}$, they possess values at ~200 $m^2\ g^{-1}$. The MW-assisted post-synthetic chemical treatment (of the parent Y) using the aqueous EDTA solution was more effective than the conventional hydrothermal treat-ment. Accordingly, MY-MW possesses the higher values of $S_{external}$ and V_{meso} (287 $m^2\ g^{-1}$ and 0.29 $cm^3\ g^{-1}$) than the MY-HT ($S_{external}$ = 205 $m^2\ g^{-1}$ and V_{meso} = 0.21 $cm^3\ g^{-1}$). Interestingly, both MY-MW and MY-HT possesses slightly higher BET surface areas (S_{BET} = 865 and 854 $m^2\ g^{-1}$, respectively) than the parent Y (S_{BET} = 817 $m^2\ g^{-1}$), indicating the well preservation of the intrinsic zeolite structure and development of mes-oporous structures by the post-synthetic modifications. Considering the treatment time of the two post treatment methods, the benefit of using MW irradiation for dealumination is obvious, *i.e.* more mesoporosity was created by a significantly reduced time (*i.e.* 1 min) than the con-ventional hydrothermal treatment (which was performed for 6 h).

Micropore and mesopore size distributions (PSDs) of the MY zeolites and the parent Y zeolite are shown in Fig. 4. Micropore PSDs of all ze-olites (Figs. 4a and b) show the mean distribution centred at around 0.74 nm which is the intrinsic micropore size of zeolite Y. Mesopore PSDs (Figs. 4c and 4d) show the distribution of well-developed mesopores in a range of 2–20 nm for MY-NCC, MY-HY and MY-MW zeolites while mesopores in MY-CNTs centres at around 20 nm, being less significant.

SEM and TEM analyses were performed to examine the morpholog-ical and microscopic properties of the materials. SEM micrograph of the parent Y (Fig. 5a) shows octahedral crystals with smooth surface, sharp edges and crystal size of *ca.* 2.5 μm. The templating methods produced MY zeolites with the spherical morphology (Fig. 5b, c andd). MY-CNTs and MY-NCC particles are the assemblies of small crystals with indi-vidual crystal sizes of 200–500 nm. These spherical assemblies of MY-CNTs and MY-NCC have varied sizes, but for MY-NCC the particle size is relatively uniform, *i.e.* about 300 nm (as shown in Figs. 5c and d). Generally, the morphology of MY-HT and MY-WM zeolites is compara-ble to that of the parent Y (Fig. 5e and f). However, surface damages are obvious in some crystals of the MY-HT and MY-WM zeolites, which might be caused by the dissolution of materials during the post

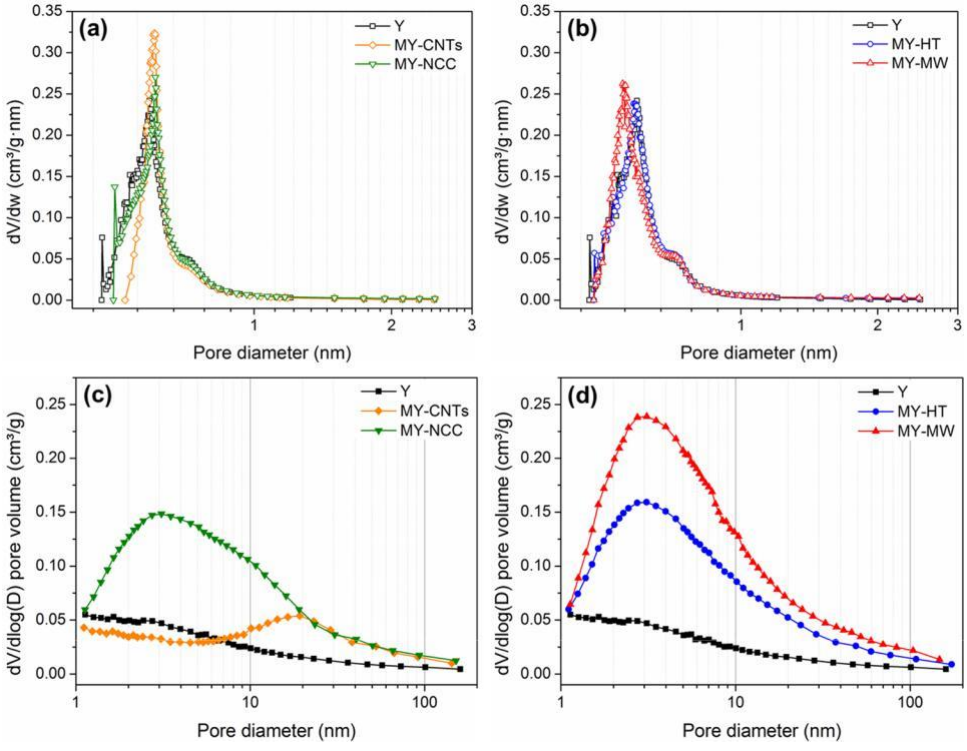

Fig. 4. Micropore PSDs by the Horvath´-Kawazoe (HK) method for (a) the MY zeolites prepared by the templating methods and (b) the MY zeolite prepared by the post-synthetic treatments; mesopores PSDs by the Barrett-Joyner-Halenda (BJH) method for (c) the MY zeolites prepared by the templating methods and (d) MY zeolite prepared by the post-synthetic treatments.

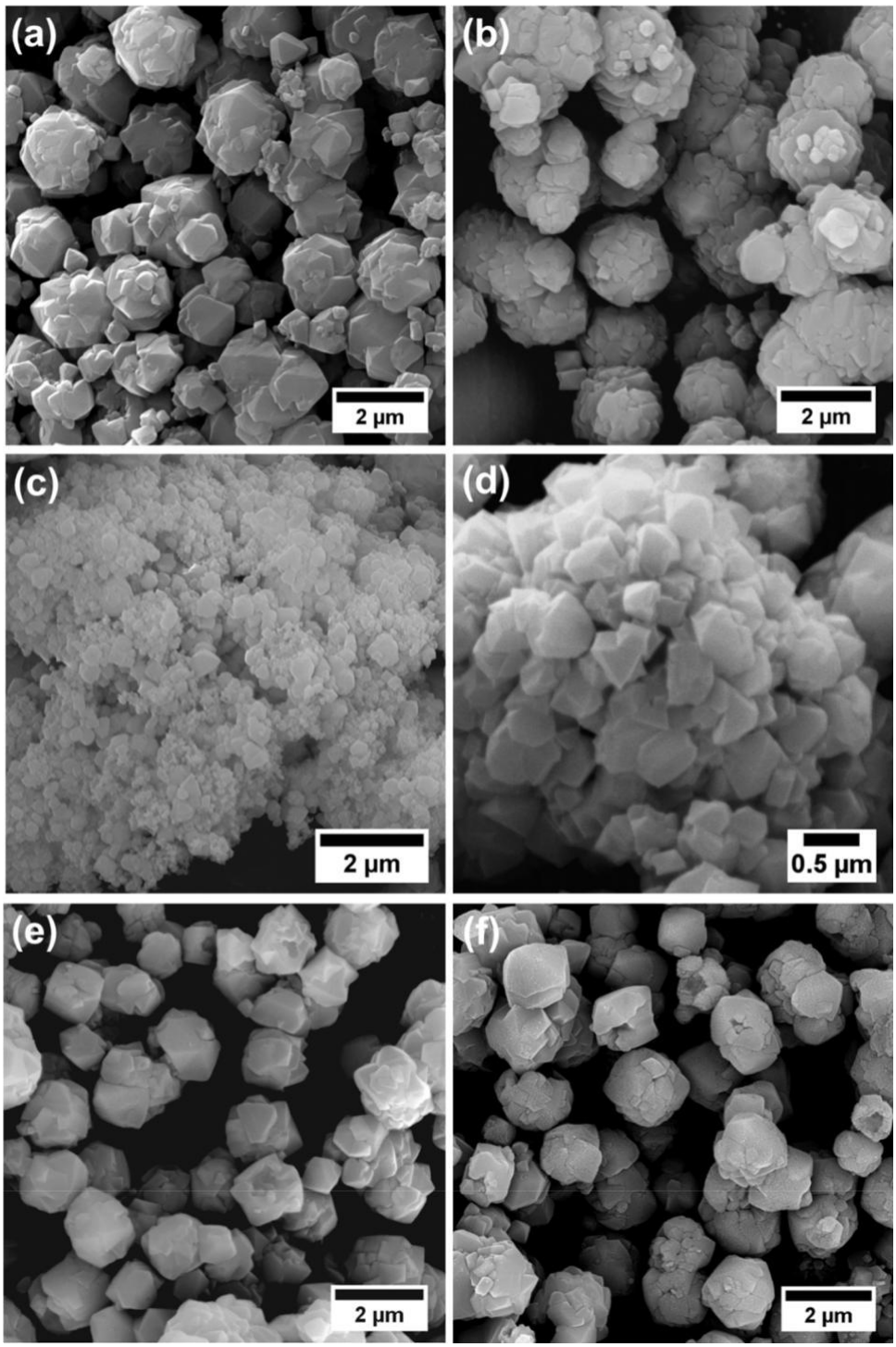

Fig. 5. SEM micrographs for (a) the parent Y, (b) MY-CNTs, (c) and (d) MY-NCC, (e) MY-HT and (f) MY-MW zeolites.

treatments of the parent Y.

HRTEM analysis (Fig. 6) enabled a close observation of microscopic features of the parent and MY zeolites. The individual crystal of the parent Y, MY-CNTs and MY-NCC zeolites show the typical dense zeolite crystalline phase with well-aligned lattice fringes (as shown in Figs. 6a–6d). By applying the Fourier Transform function (FFC) to HRTEM images (insets in Figs. 6a, 6b and 6d), the corresponding sym-metry of the lattice fringes on the HRTEM images of the samples are clear. With a low magnification (Fig. 6c), MY-NCC particles were confirmed as assemblies of nanosized Y crystals, being in line with the previous findings [19]. Therefore, the mesoporosity measured by the N_2 physisorption analysis was attributed to the intercrystal voids within the assemblies. In MY-HT and MY-MW (Fig. 6e and 6f), the characteristic intracrystalline mesoporous feature was noticeable, especially MY-MW. The bright areas across their crystalline phase represent the presence of mesopores, which allow the improved electron beam transmission. The main phase of the MY-HT and MY-MW is still crystalline, as shown by the lattice fringes in Figs. 6e and f and the relevant selected area electron diffraction (SAED) patterns (insets in Figs. 6e and f).

Acidic properties of the H-form zeolites were analysed by NH_3-TPD, as shown in Fig. 7. NH_3-TPD spectra for all the Y zeolites exhibit the typical ammonia desorption feature which can be deconvoluted into two

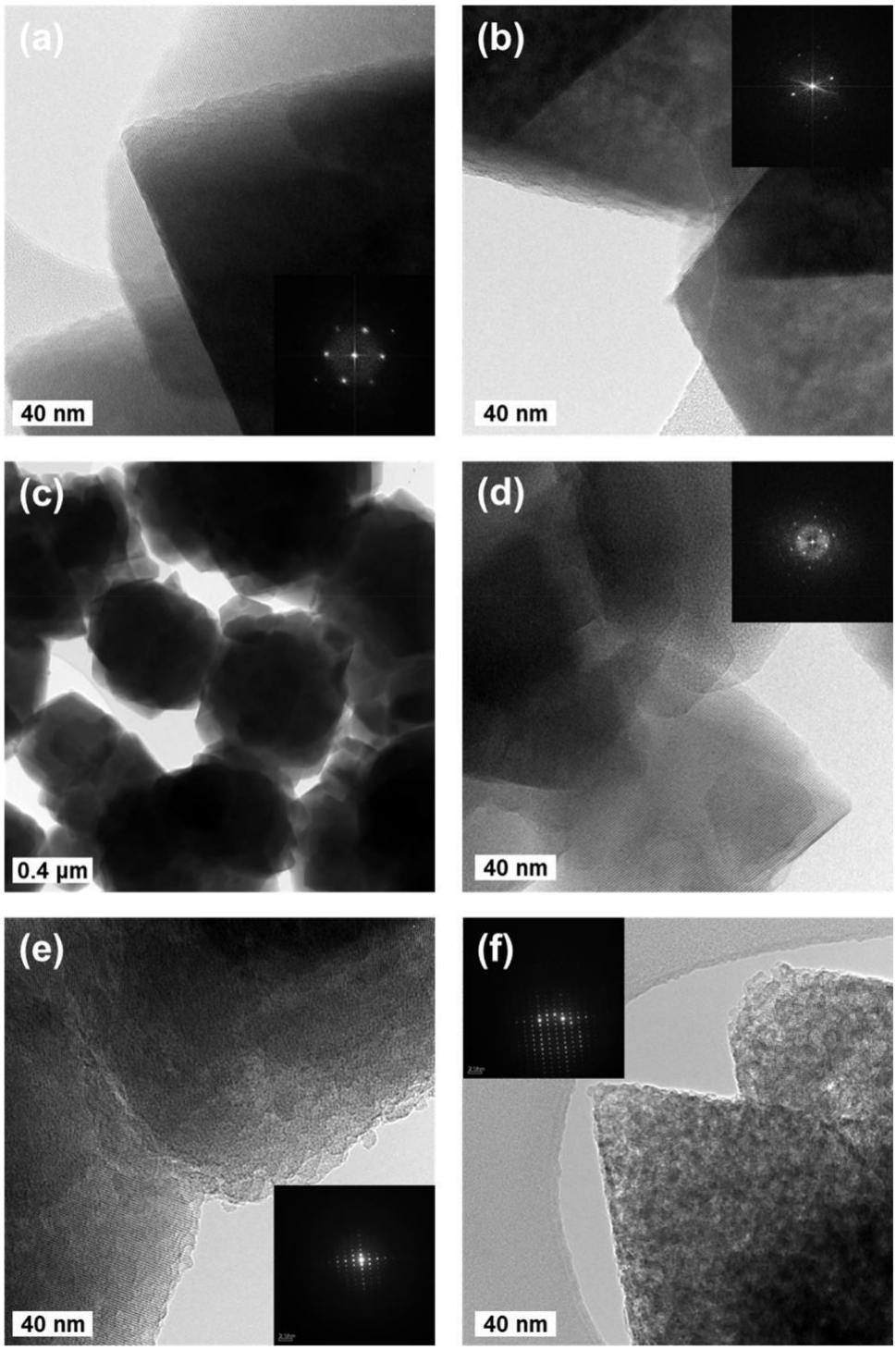

Fig. 6. HRTEM micrographs for (a) the parent Y, (b) MY-CNTs, (c) and (d) MY-NCC, (e) MY-HT and (f) MY-MW zeolites. Insets: the corresponding fast Fourier transform (FFT) of HRTEM for (a)–(d) and the selected area electron diffraction (SAED) patterns for (e)–(f).

peaks at about 200 ◦C and 300 ◦C, corresponding to its weak and strong acid sites, respectively. The low temperature peak at ~200 ◦C can be attributed to the desorption of weakly bound ammonia on zeolites (likely the weak Lewis acid sites). The high temperature peak at 300 ◦C corresponds to the ammonia desorption from the Bronested¨ acid sites [34–36]. The calculated acid site concentrations (according to the amount of ammonia desorbed from the two temperatures) were listed in Table 2, showing the insignificant variations in the strong acidity con-centration of the zeolites (*i.e.* 0.29 ± 0.05 mmol g^{1}).

3.2. Catalytic cracking performance of the zeolite catalysts

In order to probe the catalytic effectiveness of the MY zeolites under study, catalytic cracking of 1,3,5-triisopropylbenzene (TiPBz), that is, a typical model molecule of bulky aromatic for researching the catalytic cracking reactions over FCC catalysts [4,19,35,37–40], was chosen to investigate their catalytic and anti-coking properties.

Fig. 8a shows the comparison of the absolute conversions of TiPBz over the Y and MY zeolites under investigation. In details, the pristine Y zeolite promoted the initial conversion of ~71%, then rapidly

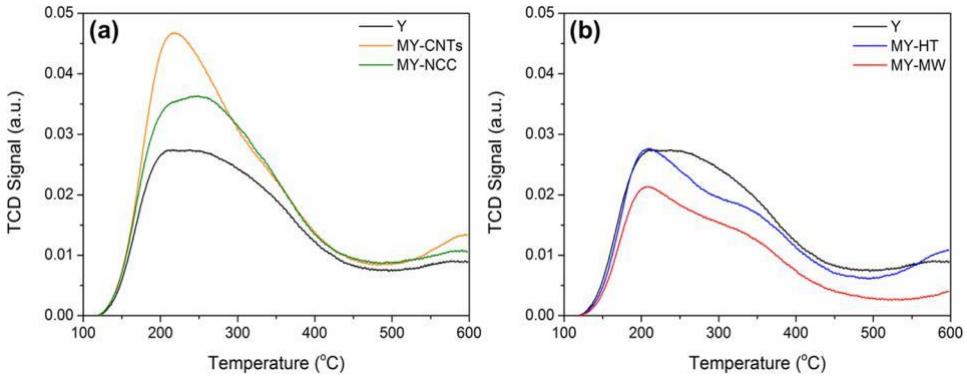

Fig. 7. NH_3-TPD curves of (a) the MY zeolites prepared by the templating methods and (b) the MY zeolites prepared by the post-synthetic treatments in reference to the parent Y.

Table 2
Acidic properties of the prepared Y and MY zeolites by NH_3-TPD.

Sample	Temperature at maximum [- C]		Weak acidity [mmol g ^{1}]	Strong acidity [mmol g ^{1}]	Total acidity [mmol g ^{1}]
	First peak	Second peak			
Y	201	309.4	0.297	0.315	0.612
MY-CNTs	213.5	317.7	0.553	0.289	0.842
MY-NCC	202.7	292.3	0.301	0.368	0.669
MY-HT	205.7	328	0.290	0.234	0.524
MY-MW	201.9	310.7	0.190	0.246	0.436

deactivated to only ~6% after 17 pulses. Comparatively, MY-CNTs was the least active catalyst and deactivated as well during the catalytic test (concerning the absolute TiPBz conversion), dropping gradually from 37% to 9%. The cracking reactions may be affected by both acidic and porous properties of zeolites. Although MY-CNTs has better mesoporous features than the pristine Y zeolite, the pristine Y zeolite possesses relatively high strong acidity (0.315 mmol g ^{1}) than MY-CNTs (0.289 mmol g ^{1}). Therefore, it is likely that the strong acidic sites of the pristine Y zeolite were more accessible (i.e. on the external surface of zeolite crystals) as compared with MY-CNTs, and hence leading to the comparatively high activity. In comparison, MY-NCC showed a better catalytic activity than the parent Y and MY-CNTs zeolites, with the initial 92% TiPBz conversion (the 1st pulse) then stabilised at about 46.7

± 4.3% (after the 8th pulse), suggesting the relatively improved anti-deactivation ability of MY-NCC than the parent Y and MY-CNTs zeo-lites. The MY zeolites prepared by the post-synthetic methods exhibited much better activity in cracking of TiPBz than their counterparts pre-pared by the hard-templating methods and the parent Y. As shown in Fig. 8a, MY-HT promoted the TiPBz conversion at 95 % at the first pulse, then slowly deactivated to 65% after the 17th pulses, while MY-MW showed the remarkable catalytic performance with >90% TiPBz con-versions during the tests, being the best catalyst among the Y and MY zeolites under study regarding the anti-deactivation property.

Generally, both acidity and porosity of zeolites are equally important to cracking reactions. However, with a bulky probing molecule, the cracking of TiPBz with three isopropyl groups requires the catalysts with the accessible acidic sites [37,41], and the accessibility to the acidic sites depends on the porous structure of the zeolite catalysts. Decoupling the two factors (*i.e.* acidic sites and hierarchical porous structure) is chal-lenging. Based on the findings by NH_3-TPD, the sequence of total acidity in the Y zeolites under study is MY-CNTs > MY-NCC > Y > MY-HT > MY-MW. TiPBz has a critical diameter of 0.95 nm [18] which is larger than the intrinsic pore width of FAU Y (*i.e.* 0.74 nm) [42], suggesting the external surface area ($S_{external}$) of the catalysts will play a significant role in promoting the cracking of alkyl groups. Therefore, based on the assumption of (*i*) the even distribution of all acidic sites throughout the pore surface (including both $S_{external}$ and S_{micro}) and (*ii*) insignificant conversion of TiPBz in the microporous domain, the absolute conversion of TiPBz can be normalised based on the concentration of total acidic sites on the external surface of the zeolite ($X_{acidity@ext.}$) according to Eq.
3 [19].

$$X_{acidity@ext.} = X \Big/ C_{total\ acidity} \cdot M \cdot \left(\frac{S_{external}}{S_{BET}}\right) \quad (3)$$

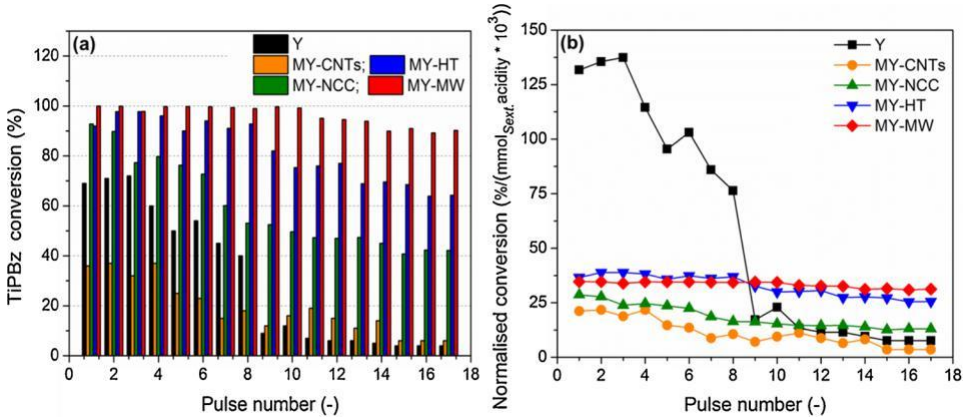

Fig. 8. (a) Absolute conversion and (b) normalised conversion of TiPBz over the parent Y, MY-CNTs, MY-NCC, MY-HT and MY-MW zeolite catalysts as a function of the pulse number.

where, $X_{acidity@ext.}$ is the normalised conversion based on the meso-porous feature of zeolites [% mmol 1], X is the absolute TiPBz conver-sion [%], $C_{total\ acidity}$ is the measured concentration of the total acidity by NH[g].3 - TPD [mmol g ^{1}] and M is the mass of the zeolite used in catalysis Based on the assumptions above, the comparison of the normalised conversions (Fig. 8b) shows that, at the initial stage of the catalytic evaluation (pulse number <8), the parent Y was more effective than the MY zeolites, *i.e.* about four folds, indicating that the readily accessible external surface area of Y (or the external crystal surface) contributed to the cracking reactions. However, the parent Y deactivates fast which might be due to coke deposition on the crystal surface, highlighting the intrinsic drawback of the microporous zeolite. For Y zeolites with the mesoporous features (*i.e.* MY zeolites), they demonstrated relatively stable performance regarding the normalised conversion. Considering the change of the normalised conversion as a function of the pulse number, the deactivation rate (*i.e.* the difference between the initial and the final normalised conversion divided by the initial normalised con-version) of mesoporous MY zeolites can be ranked as: MY-MW (9.8%) < MY-HT (30.2%) < MY-NCC (54.5%) < MY-CNTs (83.3%), being lower than that of the parent Y (*ca.* 94.2%). Specifically, MY-MW shows the most stable performance over the course of catalytic tests, which could be attributed to the presence of abundant intracrystalline mesoporosity, promoting an excellent molecular diffusion to and from the acidic sites. Interestingly, although MY-HT was measured with a lower amount of external surface area than MY-MW (Table 1), it showed relatively higher normalised conversion during the initial injections (pulse number <9). Afterwards, MY-HT deactivated gradually, giving a deactivation rate of ~30.2%. The findings indicate that the mesoporosity in MY-HT might not be as hierarchical as that in MY-MW. Therefore, the initial high activate can be mainly ascribed to the reaction on the external crystal surface rather than on the external surface of the intracrystalline mes-oporous network.

Regarding the MY zeolites with the intercrystal mesoporosity, *i.e.* MY-CNTs and MW-NCC, steady deactivation was measured, and the rate correlated with the level of intercrystals mesoporosity they possess. This is reasonable, since their particles are assemblies of small size micro-porous zeolite crystals, and hence in this case the external crystal surface of nanozeolites contributes to the external surface area measured by N_2 physisorption as whole for the assemblies.

Previously, the main catalytic products of TiPBz were reported as propylene, benzene, toluene, xylene (including *para*, *meta*, *ortho* xylene),

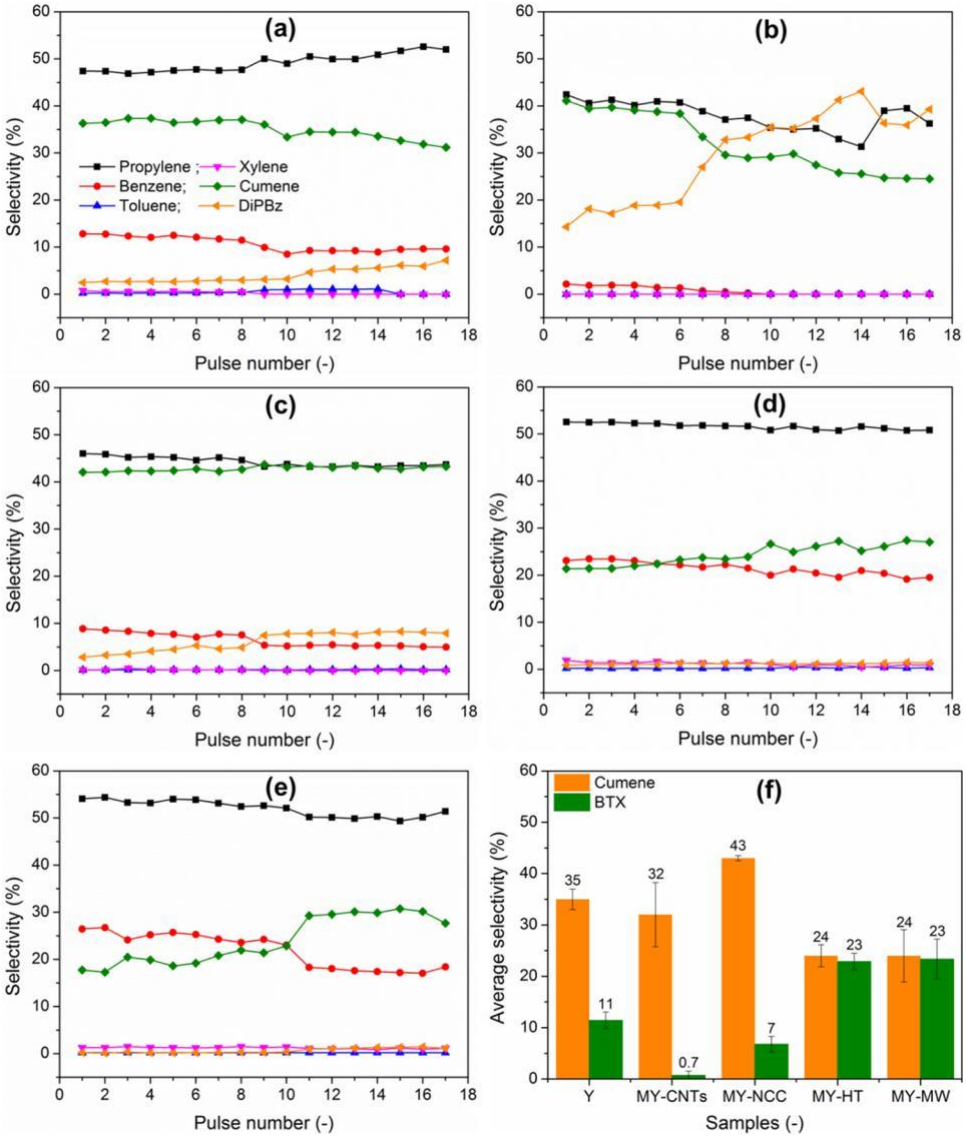

Fig. 9. Product selectivity of catalytic cracking of TiPBz over (a) parent Y, (b) MY-CNTs, (c) MY-NCC, (d) MY-HT and (e) MY-MW zeolites; (f) average selectivity (to cumene and BTX) over the zeolite catalysts.

cumene and diisopropyl benzene (DiPBz) (including 1,3 and 1,4 DiPBz) [43–46]. The detailed analysis of the selectivity to different cracking products by this work is presented in Fig. 9. The mechanism of TiPBz cracking over zeolites is the dealkylation of isopropyl groups by the acidity. Therefore, the intrinsic selectivity of the zeolites under study is similar, and the difference in the selectivity of the zeolites (Fig. 9) can be principally due to the effect of their textural properties. MY-HT and MY-MW zeolites with intracrystalline mesoporosity promoted the se-lectivities to propylene, benzene and cumene, at ~98%, which are higher than the parent Y (~94%), MY-CNTs (~62%) and MY-NCC (~95%), suggesting more complete cracking reactions. Cumene is an intermediate from the TiPBz cracking due to the dealkylation of two isopropyl groups from TiPBz, and BTX (benzene, toluene, and xylene) can be considered as the final aromatic hydrocarbon products of the complete cracking of TiPBz. Therefore, the consideration of the average selectivity to BTX and cumene enables the analysis of the effectiveness of the parent and MY zeolites, as shown in Fig. 9f. Again, both MY-HT and MY-MW zeolites gave the highest average selectivity toward BTX (~23%) and the lowest average selectivity toward cumene at ~24%. Comparably, MY-CNTs showed the poorest performance with about 43% selectivity to cumene and 0.7% selectivity to BTX, meaning the successive cracking of the intermediate during TiPBz cracking is difficult over it. This also applies to the parent Y and MY-NCC with the average selectivity to cumene at 35% and 32%, and BTX at 11% and 7%, respectively.

The product yields are shown in Fig. 10. In general, Y-MW and MY-HT with intracrystalline mesoporosity shows higher overall yields of propylene, benzene and cumene (with the favour to propylene and benzene) than the parent Y, NY-NCC, MY-CNTs, suggesting that hierarchical feature of intracrystalline mesoporosity in the two zeolites, especially MY-MW, improves the accessibility to and diffusion in their zeolite frameworks.

Based on the findings of the catalytic tests in this comparative study, one can conclude that (*i*) the post-synthetic treatments are more bene-ficial than the templating methods to develop mesoporous zeolite Y for cracking reactions and (*ii*) the hierarchical mesopores improves the framework accessibility, facilitating a stable performance in catalysis. Comparatively, the microwave-assisted post-synthetic treatment (*i.e.* the MWAC method) delivered the hierarchical mesoporous Y zeolite which was supported by the characterisation and catalytic evaluation. Post-reaction TGA of the used zeolite catalysts gives the estimation of coke deposition due to the cracking reaction, and the relevant TG curves are presented in Fig. 11. By comparing the weight loss of the used zeolites in the region of 100–600 °C, the following order of weight loss was

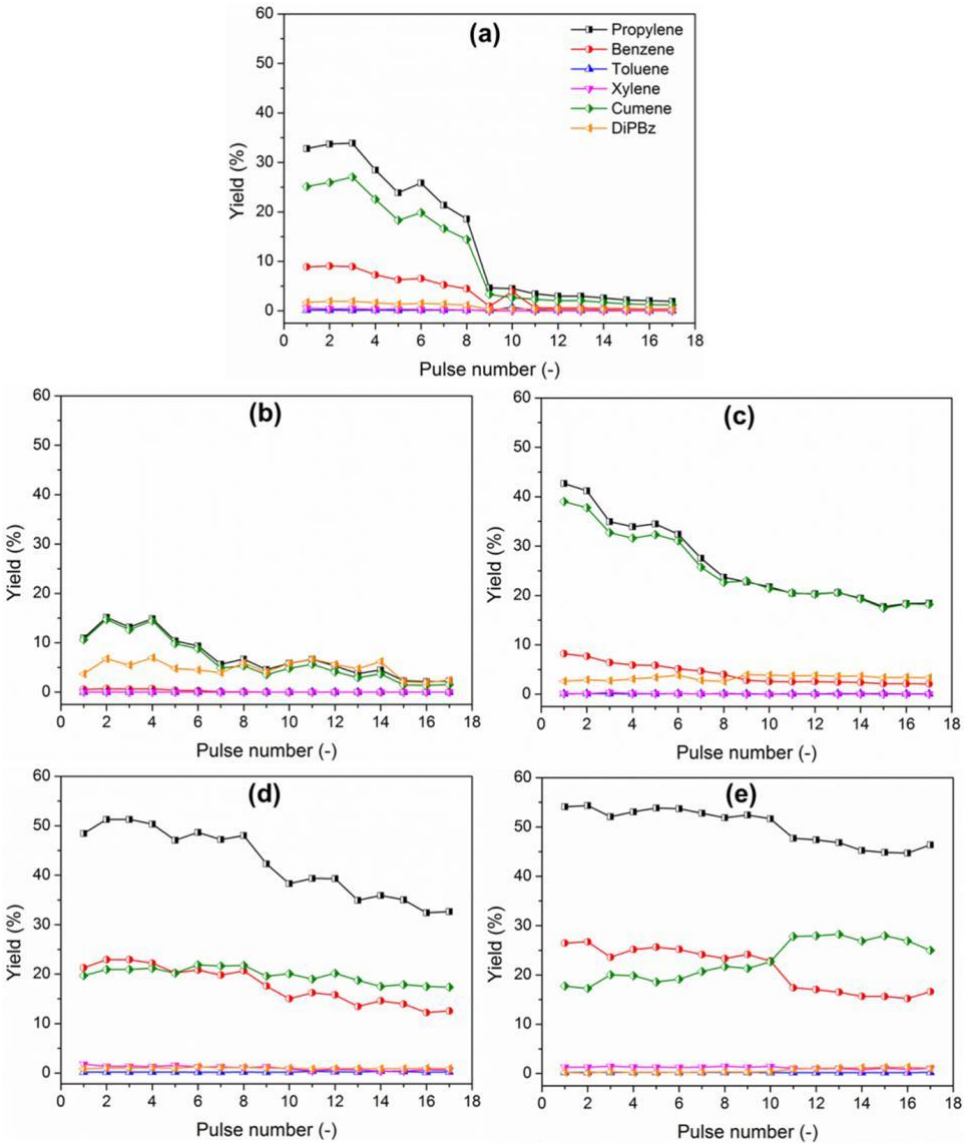

Fig. 10. Product yield of TiPBz cracking over (a) parent Y, (b) MY-CNTs, (c) MY-NCC, (d) MY-HT and (e) MY-MW zeolites.

obtained: MY-MW (6.2%) < MY-HT (8.5%) < MY-NCC (9.5%) < MY-CNTs (10.8%) < parent Y (12%). The findings by TGA are in line with the previous discussion on catalysis, proving the anti-coking ability due to the presence of mesoporosity, as well as the advantage of the intra-crystalline mesoporosity than the intercrystal mesoporosity. Compared with MY-NCC, the coke deposition in MY-MW was reduced by about 35%.

3.3. Preliminary economic analysis

The preliminary economic analysis was performed (in reference to the parent Y zeolite) to gain some insights into the cost aspect of the four methods employed for the laboratory-scale production of MY zeolites. The analysis took into account the retail costs of materials and chemicals used for zeolite synthesis and modification, as well as the relevant en-ergy consumption of the synthesis and post-treatment processes. In detail, the analysis of the parent Y, MY-NCC and MY-CNTs zeolites only considered the energy consumption for the HT synthesis because the templating methods only involved the addition of hard templates during the routine HT synthesis without changing other process parameters (e. g., temperature). The analysis of MY-HT and MY-MW zeolites included the additional energy required for post-synthetic treatments (i.e., deal-umination under the MW and HT conditions and desilication under the HT condition). Since the same calcination procedure was used for all zeolites under investigation, the associated costs were not included in the analysis. Relevant details of the calculations are presented in SI.

Based on the current method at the laboratory-scale, the preparation of 1 g parent Y zeolite costed £0.56 with the majority (*ca.* 82%) from the energy consumption, as shown in Fig. 12. The cost of energy con-sumption was calculated by multiplying the power consumed (kilowatt hour, kWh) with the rate (pence, P, kWh ^{1}), where the power was recorded by a plug-in power meter during the preparation and the rate of 13.85 P kWh ^{1} was obtained from the average annual standard elec-tricity bills in the UK with average unit costs (quarterly energy prices report) [47]. The production of 1 g of MY-NCC and MY-CNTs required the cost at £0.61 and £0.84, respectively. As discussed above, the tem-plating synthesis methods were similar to that for preparing the parent Y zeolite, and thus the additional cost of MY-CNTs and MY-NCC was mainly due to the cost of hard templates. In comparison with CNTs, NCC was much more economic with the retail cost at only ~1.3% of CNTs. Additionally, CNTs also required oxidation treatment (using NaOCl so-lution) before being used as the template, which increased the cost of materials (about 40% of the £0.84). Considering the sustainable and renewable features of NCC, as well as its capability to facilitate the bottom-up synthesis of mesoporous Y zeolites, NCC shows the potential (regarding the sustainability and cost effectiveness) for further

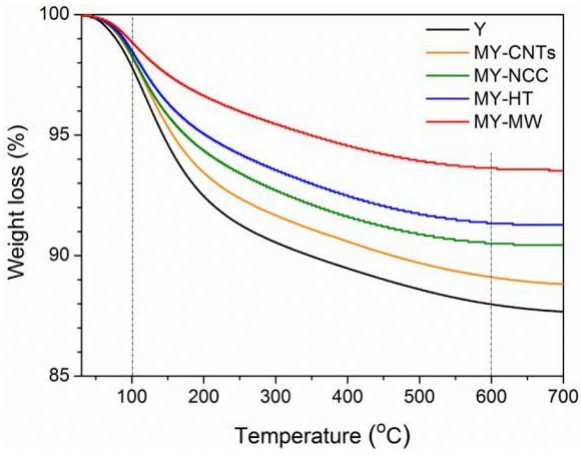

Fig. 11. TG curves of the used parent Y and MY zeolites from the pulse ex-periments in catalytic cracking of TiPBz at 325 ◦ C.

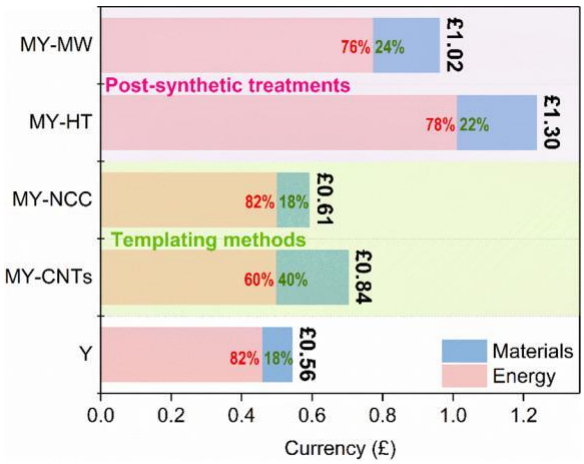

Fig. 12. Estimated costs of Y and MY zeolites prepared by this work based on the laboratory-scale production of 1 g of the relevant materials.

exploration at large scales, particularly from an industrial perspective. The top-down approaches required the use of relevant chemicals and additional energy during the post-synthetic treatments, which added extra costs on the MY-HT and MY-MW zeolites. As a result, the pro-duction cost of making 1 g MY-MW and MY-HT was estimated at £1.02 and £1.30, respectively. By comparing the energy required by the post-synthetic dealumination treatments, the MW-assisted dealumination treatment was highly energy efficient. In comparison with the conven-tional HT dealumination, the MW treatment only consumes 0.05 kW h of electricity in minutes, whereas the HT treatment consumes roughly 1.05 kW h in 6 h. Therefore, comparatively, the MW method can be energy-and cost-effective for preparing mesoporous zeolites with the well-developed intracrystalline mesoporosity. In summary, by comparing the estimated total costs of the zeolite materials under investigation, the templating methods, especially the one employing the NCC template, were relatively attractive regarding the production costs (on the laboratory-scale). Conversely, although they are comparatively expen-sive methods, the post-synthetic treatments were much more effective to produce intracrystalline mesoporosity, which could benefit the cracking catalysis. Therefore, the trade-off between costs and catalytic perfor-mance of mesoporous zeolites needs to be considered comprehensively in future studies.

4. Conclusions

A systematic and comparative study of mesoporous Y (MY) zeolites prepared by the templating (bottom-up) and post-synthetic treatment (top-down) methods was performed (in reference to the parent Y zeolite from the same origin). Specifically, the bottom-up approaches were enabled using carbon nanotubes (CNTs) and nanocrystalline cellulose (NCC) as the templates, and the top-down methods employed the sequential microwave-assisted and hydrothermal chemical treatment (for dealumination) and alkaline treatment (for desilication). The mes-oporosity, acidity and catalytic activity (in the model cracking catalysis) of the MY and Y zeolites were compared and discussed in detail. Based on the findings of characterisation and catalysis, it is found that the top-down methods are comparatively beneficial than the bottom-up ap-proaches to make mesoporous Y zeolites. Especially, the post-synthetic dealumination facilitated by the microwave irradiation was highly effective and efficient to produce the intracrystalline mesoporosity (*i.e.* the external surface area of 287 m^2 g^{1} without compromising the relative crystallinity to a large extent), being superior to other meso-porous Y zeolites developed by this work, and thus contributing to the catalysis.

In the templating strategy for making mesoporous Y zeolites, NCC as

the template was much more effective than the CNTs in producing the intercrystal mesoporosity with the relatively high mesopore volume of 0.21 $cm^3\ g^{-1}$ and external surface area of 197 $m^2\ g^{-1}$. According to the catalytic results (*i.e.* the catalytic cracking of 1,3,5-triisopropylbenzene, TiPBz), the mesoporous Y zeolites with the intracrystalline mesoporosity (*i.e.* the MY-MW and MY-HT) showed the comparatively better catalytic and anti-deactivation performance than the mesoporous Y zeolites prepared by the bottom-up templating methods (*i.e.* the MY-CNTs and MY-NCC with the intercrystal mesoporosity). By normalising the abso-lute conversion of TiPBz using the total acidity concentration on the external surface area, it was found that the accessible intracrystalline mesoporosity is preferred than the intracrystal mesoporosity for pro-moting a better cracking catalysis, resulting in the high selectivity to-wards valuable light olefins and BTX components. The preliminary economic analysis was performed to estimate the cost aspects of pre-paring the MY zeolites at the laboratory scale, suggesting that the NCC templating method and the microwave assisted post-synthesis treatment deserve the further exploitation with industrial relevance.

CRediT authorship contribution statement

Samer Abdulridha: Data curation, Writing - original draft. **Yilai Jiao:** Data curation, Methodology. **Shaojun Xu:** Data curation. **Rongxin Zhang:** Data curation. **Zhongyuan Ren:** Data curation, Writing - review & editing. **Arthur A. Garforth:** Writing - review & editing. **Xiaolei Fan:** Conceptualization, Writing - review & editing, Supervision.

Declaration of Competing Interest

The authors report no declarations of interest.

Acknowledgements

S.A. was supported by The Higher Committee for Education Development in Iraq via a postgraduate research scholarship at The University of Manchester. Y.J. and X.F. thanks the financial support from the Key Project on Intergovernmental International Science, Technology and Innovation (STI) Cooperation/STI Cooperation with Hong Kong, Macao and Taiwan of China's National Key R&D Programme (2019YFE0123200). R.Z. thanks the financial support by the Education Bureau Project of Jilin Province (Grant No. JJKH20200246KJ) for his research and collaboration.

Appendix A. Supplementary data

References

[1] R. Chal, C. Gerardin,´ M. Bulut, S. van Donk, ChemCatChem 3 (2011) 67–81.
[2] D. Verboekend, J. Perez-Ramirez, ChemSusChem 7 (2014) 753–764.
[3] Y. Wei, T.E. Parmentier, K.P. de Jong, J. Zecevic, Chem. Soc. Rev. 44 (2015) 7234–7261.
[4] J.-P.G. Hussein Awala, Richard Retoux, Philippe Boullay, Jean-Michel Goupil, V.V. a.S. Mintova, Nat. Mater. 14 (2015) 447–451.
[5] D. Verboekend, N. Nuttens, R. Locus, J. Van Aelst, P. Verolme, J.C. Groen, J. P´erez-Ramírezc, B.F. Selsa, Chem. Soc. Rev. 45 (2016) 3331–3352.
[6] U.J. Etim, B.J. Xu, Z. Zhang, Z.Y. Zhong, P. Bai, K. Qiao, Z.F. Yan, Fuel 178 (2016) 243–252.
[7] J.O. Abildstrom, Z.N. Ali, U.V. Mentzel, J. Mielby, S. Kegnaes, M. Kegnaes, New J. Chem. 40 (2016) 4223–4227.
[8] D. Verboekend, G. Vil´e, J. Perez´-Ramírez, Adv. Func. Mater. 22 (2012) 916–928.
[9] A. Sachse, C. Wuttke, U. Díaz, M.O. de Souza, Microporous Mesoporous Mater. 217 (2015) 81–86.
[10] J. Zhao, Y. Yin, Y. Li, W. Chen, B. Liu, Chem. Eng. J. 284 (2016) 405–411.
[11] M. Qamar, I. Baig, A.M. Azad, M.I. Ahmed, M. Qamaruddin, Chem. Eng. J. 290 (2016) 282–289.
[12] C. Manrique, A. Guzman,´ J. P´erez-Pariente, C. Marquez´-Alvarez,´ A. Echavarría, Fuel 182 (2016) 236–247.
[13] B. Meng, S. Ren, Z. Li, H. Duan, X. Gao, H. Zhang, W. Song, Q. Guo, B. Shen, ACS Appl. Nano Mater. 3 (2020) 9293–9302.
[14] Y. Qiu, L. Wang, X. Zhang, G. Liu, RSC Adv. 5 (2015) 78238–78246.
[15] Y.S. Tao, H. Kanoh, K. Kaneko, J. Phys. Chem. B. 107 (2003) 10974–10976.
[16] Y. Zhang, K. Zhu, X. Duan, P. Li, X. Zhou, W. Yuan, RSC Adv. 4 (2014) 14471–14474.
[17] J. Zhao, G. Wang, L. Qin, H. Li, Y. Chen, B. Liu, Catal. Commun. 73 (2016) 98–102.
[18] Y. Jiao, L. Forster, S. Xu, H. Chen, J. Han, X. Liu, Y. Zhou, J. Liu, J. Zhang, J. Yu, C. D'Agostino, X. Fan, Angew. Chem. Int. Ed. 59 (2020) 19478–19486.
[19] S. Abdulridha, J. Jiang, S. Xu, Z. Zhou, H. Liang, B. Mao, Y. Zhou, A.A. Garforth, Y. Jiao, X. Fan, Green Chem. 22 (2020) 5115–5122.
[20] J. P´erez-Ramírez, S. Abello,´ A. Bonilla, J.C. Groen, Adv. Func. Mater. 19 (2009) 164–172.
[21] J. García-Martínez, M. Johnson, J. Valla, K. Li, J.Y. Ying, Catal. Sci. Technol. 2 (2012) 987–994.
[22] S. Abdulridha, Y. Jiao, S. Xu, R. Zhang, A.A. Garforth, X. Fan, Front. Chem. 8 (2020) 482.
[23] R. Zhang, D. Raja, Y. Zhang, Y. Yan, A.A. Garforth, Y. Jiao, X. Fan, Top. Catal. 63 (2020) 340–350.
[24] R. Zhang, P. Zhong, H. Arandiyan, Y. Guan, J. Liu, N. Wang, Y. Jiao, X. Fan, Front. Chem. Sci. Eng. 14 (2020) 275–287.
[25] Z. Qin, W. Shen, S. Zhou, Y. Shen, C. Li, P. Zeng, B. Shen, Microporous Mesoporous Mater. 303 (2020), 110248.
[26] S. Abdulridha, R. Zhang, S. Xu, A. Tedstone, X. Ou, J. Gong, B. Mao, M. Frogley, C. Bawn, Z. Zhou, X. Zhang, S. Chansai, S.M. Holmes, C. Hardacre, A.A. Garforth, S. Yang, Y. Jiao, X. Fan, Microporous Mesoporous Mater. 311 (2021), 110715.
[27] X. Meng, F. Nawaz, F.-S. Xiao, Nano Today 4 (2009) 292–301.
[28] J. Zhou, Z. Hua, J. Shi, Q. He, L. Guo, M. Ruan, Chemistry 15 (2009) 12949–12954.
[29] L. Zhang, X. Liu, X. Li, X. Gao, H. Sui, J. Zhang, Z. Yang, C. Tian, H. Li, Chin. J. Chem. Eng. 21 (2013) 821–826.
[30] Y. Jiao, X. Fan, M. Perdjon, Z. Yang, J. Zhang, Appl. Catal. A Gen. 545 (2017) 104–112.
[31] K.S.W. Sing, D.H. Everett, R.A.W. Haul, L. Moscou, R.A. Pierotti, J. Rouquerol, T. Siemieniewska, Pure Appl. Chem. 57 (1985) 603–619.
[32] C. Chou, C.S. Cundy, A.A. Garforth, Stud. Surf. Sci. Catal. 156 (2005) 393–400.
[33] D.Z. Shen, J. Liu, L.H. Gan, N.Z. Huang, M.N. Long, RSC Adv. 7 (2017) 19237–19242.
[34] D. Wang, L. Zhang, L. Chen, H. Wu, P. Wu, J. Mater. Chem. A 3 (2015) 3511–3521.
[35] Z.X. Qin, B.J. Shen, X.H. Gao, F. Lin, B.J. Wang, C.M. Xu, J. Catal. 278 (2011) 266–275.
[36] R. Zhang, S. Xu, D. Raja, N.B. Khusni, J. Liu, J. Zhang, S. Abdulridha, H. Xiang, S. Jiang, Y. Guan, Y. Jiao, X. Fan, Microporous Mesoporous Mater. 278 (2019) 297–306.
[37] S.-R. Zhai, W. Wei, D. Wu, Y.-H. Sun, Catal. Lett. 89 (2003) 261–267.
[38] S.-R. Zhai, I. Kim, C.-S. Ha, Catal. Today 131 (2008) 55–60.
[39] Y. Choi, Y.S. Yun, H. Park, D.S. Park, D. Yun, J. Yi, Chem. Commun. 50 (2014) 7652–7655.
[40] W. Li, C. Tu, J. Zheng, Y. Luo, Z. Da, ChemistrySelect 1 (2016) 934–939.
[41] S. Zhai, Y. Zhang, D. Wu, Y. Sun, S. Wang, Top. Catal. 39 (2006) 227–235.
[42] D. Yuan, C. Kang, W. Wang, H. Li, X. Zhu, Y. Wang, X. Gao, B. Wang, H. Zhao, C. Liu, B. Shen, Catal. Sci.Technol. 6 (2016) 8364–8374.
[43] N. Al-Baghli, S. Al-Khattaf, Stud. Surf. Sci. Catal. 158 (2005) 1661–1668.
[44] A. Bazyari, A.A. Khodadadi, N. Hosseinpour, Y. Mortazavi, Fuel Process. Technol. 90 (2009) 1226–1233.
[45] T. Odedairo, R.J. Balasamy, S. Al-Khattaf, J. Mol. Catal. A Chem. 345 (2011) 21–36.
[46] M. Davoodpour, R. Tafreshi, A.A. Khodadadi, Y. Mortazavi, Korean J. Chem. Eng. 34 (2017) 681–691.
[47] Quarterly energy prices A National Statistics Publication, Department of Energy and Climate Change, 2012, pp. 1–84.